

# Journal of Materials Chemistry A

Materials for energy and sustainability

Accepted Manuscript

This article can be cited before page numbers have been issued, to do this please use: C. Wang, W. Zhou, Z. Sun, Y. Wang, B. Zhang and Y. Yu, *J. Mater. Chem. A*, 2020, DOI: 10.1039/D0TA09590G.



This is an Accepted Manuscript, which has been through the Royal Society of Chemistry peer review process and has been accepted for publication.

Accepted Manuscripts are published online shortly after acceptance, before technical editing, formatting and proof reading. Using this free service, authors can make their results available to the community, in citable form, before we publish the edited article. We will replace this Accepted Manuscript with the edited and formatted Advance Article as soon as it is available.

You can find more information about Accepted Manuscripts in the [Information for Authors](#).

Please note that technical editing may introduce minor changes to the text and/or graphics, which may alter content. The journal's standard [Terms & Conditions](#) and the [Ethical guidelines](#) still apply. In no event shall the Royal Society of Chemistry be held responsible for any errors or omissions in this Accepted Manuscript or any consequences arising from the use of any information it contains.

## COMMUNICATION

## Integrated Selective Nitrite Reduction to Ammonia with Tetrahydroisoquinolines Semi-dehydrogenation over a Vacancy-Rich Ni Bifunctional Electrode

Received 00th January 20xx,  
Accepted 00th January 20xx

DOI: 10.1039/x0xx00000x

Changhong Wang,<sup>#a</sup> Wei Zhou,<sup>#b</sup> Zhaojun Sun,<sup>b</sup> Yuting Wang,<sup>b</sup> Bin Zhang<sup>a,b</sup>, and Yifu Yu<sup>\*a</sup>

**The development of efficient electrocatalysts for nitrite reduction to ammonia, especially integrated with a value-added anodic reaction, is important. Herein, Ni nanosheet arrays with Ni vacancies (Ni-NSA-V<sub>Ni</sub>) were demonstrated to exhibit outstanding electrocatalytic performances toward selective nitrite reduction to ammonia (Faradaic efficiency: 88.9%; Selectivity: 77.2%) and semi-dehydrogenation of tetrahydroisoquinolines (Faradaic efficiency: 95.5%; Selectivity: 98.0%). The origin and quantitative analysis of ammonia were performed by <sup>15</sup>N isotope labeling and <sup>1</sup>H NMR experiments. The decrease in electronic cloud density induced by the Ni vacancies was found to improve the NO<sub>2</sub><sup>-</sup> adsorption and NH<sub>3</sub> desorption, leading to high nitrite-to-ammonia performance. *In situ* Raman results revealed the formation of Ni<sup>II</sup>/Ni<sup>III</sup> active species for anodic semi-dehydrogenation of tetrahydroisoquinolines on Ni-NSA-V<sub>Ni</sub>. Importantly, a Ni-NSA-V<sub>Ni</sub> || Ni-NSA-V<sub>Ni</sub> bifunctional two-electrode electrolyzer was constructed to simultaneously produce ammonia and dihydroisoquinoline with robust stability and high selectivity.**

Nitrite (NO<sub>2</sub><sup>-</sup>), as one of the most common contaminants in groundwater, can cause serious health problems.<sup>1-4</sup> Electrocatalytic reduction has emerged as a promising strategy to remove nitrite.<sup>5-8</sup> Simultaneously, ammonia/ammonium has been widely used in agriculture and industry.<sup>9-11</sup> Interestingly, nitrite is difficult to be recycled, while ammonia can be easily reclaimed from its aqueous solution.<sup>12, 13</sup> Thus, adopting nitrite as the nitrogen source and water as the hydrogen source to produce ammonia is promising for the artificial nitrogen cycle. Recently, a series of metal complexes as homogeneous electro-catalysts exhibited high activity for selective nitrite reduction to ammonia.<sup>14-16</sup> Considering the separation difficulties of homogeneous electrocatalyst, a heterogeneous

electrocatalyst for selective nitrite reduction to ammonia is urgently needed.

The counter reaction to nitrite reduction is the kinetically sluggish oxygen evolution reaction (OER), which requires large overpotential, and its product O<sub>2</sub> does not bear a high price tag.<sup>17</sup> An alternative strategy is to develop a thermodynamically favorable anodic reaction to produce value-added fine chemicals.<sup>18</sup> Dihydroisoquinolines (DHIQs), as an important intermediate in the pharmaceutical industry, display a wide range of bioactivities on anti-tumor, anti-fungal, vasodilation and monoamine oxidase inhibition.<sup>19</sup> DHIQs can be prepared through the dehydrogenation of tetrahydroisoquinolines (THIQs). The challenge of this reaction lies in the controlled semi-dehydrogenation of THIQs to avoid undesirable over-dehydrogenation.<sup>20-22</sup> Recently, our group reported that Ni<sub>2</sub>P could electrocatalyze semi-dehydrogenation of THIQs into DHIQs and the *in situ* formed Ni<sup>II</sup>/Ni<sup>III</sup> redox served as the active species.<sup>23</sup> But, expensive phosphorus source or/and dangerous gaseous PH<sub>3</sub> byproducts are the big concerns for the synthesis of Ni<sub>2</sub>P nanostructures.<sup>23-25</sup> Pure Ni is one of the cheap Ni-based materials, but its electrocatalytic performance is low. Interestingly, introducing anion or cation vacancies into materials could regulate their electronic structures to improve electrocatalytic performances.<sup>26-33</sup> However, Ni nanostructures with Ni vacancies are rarely touched due to the wet-chemical synthetic difficulty. Therefore, the development of a facile method to synthesize nickel with rich Ni vacancies as a bifunctional electrocatalyst for integrating semi-dehydrogenation of THIQs with selective nitrite electroreduction to ammonia is significant but still remains a great challenge.

Here, Ni nanosheet arrays with Ni vacancies, denoted as Ni-NSA-V<sub>Ni</sub>, were prepared through plasma-assisted synthesis and exhibited high performance for selective nitrite electroreduction and semi-dehydrogenation of THIQs. The experimental and density functional theory (DFT) calculation results revealed that Ni vacancies promoted the conversion from nitrite to ammonia. *In situ* Raman spectra confirmed the formation of Ni<sup>II</sup>/Ni<sup>III</sup> active species for semi-dehydrogenation

<sup>a</sup> Institute of Molecular Plus, Tianjin University, Tianjin 300072, China.

<sup>b</sup> School of Science, Key Laboratory of Molecular Optoelectronic Sciences, Tianjin University, Tianjin 300072, China.

<sup>#</sup> These authors contributed equally to this work.

Electronic Supplementary Information (ESI) available: Experimental details, supplementary characterization and electrochemical measurements. See DOI: 10.1039/x0xx00000x

## COMMUNICATION

of THIQs. Ni-NSA-V<sub>Ni</sub> could act as efficient bifunctional electrodes for simultaneously producing ammonia and DHIQs with high stability and selectivity in a Ni-NSA-V<sub>Ni</sub> || Ni-NSA-V<sub>Ni</sub> two-electrode electrolyzer.

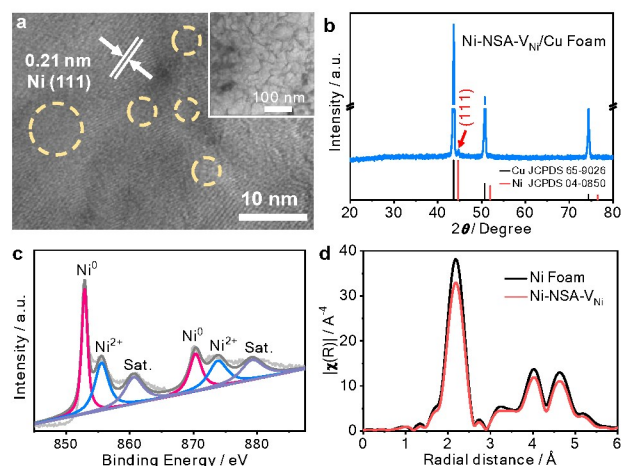


**Figure 1.** (a) HRTEM image of Ni-NSA-V<sub>Ni</sub>. Inset is the corresponding TEM image. (b) XRD pattern of Ni-NSA-V<sub>Ni</sub>/Cu Foam. (c) XPS spectra of Ni-NSA-V<sub>Ni</sub>. (d) Ni K-edge radial structure functions of Ni Foam and Ni-NSA-V<sub>Ni</sub>.

Ni-NSA-V<sub>Ni</sub> were synthesized through a facile H<sub>2</sub>-plasma chemical conversion (see the Supporting Information for details). First, Ni(OH)<sub>2</sub> nanosheets array supported on Ni foam were prepared by a typical solution-chemical method (Figure S1) and then reduced into Ni nanosheet arrays (Ni-NSA) by ethylene glycol.<sup>34</sup> Finally, Ni-NSA-V<sub>Ni</sub> could be obtained through the H<sub>2</sub>-plasma treatment on Ni-NSA because of the etching role of plasma. A series of advanced techniques were adopted to characterize Ni-NSA-V<sub>Ni</sub>. Scanning electronic micrograph (SEM) images (Figure S2a,b) showed the nanosheet array morphology of Ni-NSA and Ni-NSA-V<sub>Ni</sub>, suggesting the morphology retention during the plasma-assisted conversion synthesis. Transmission electronic micrograph (TEM) image of Ni-NSA-V<sub>Ni</sub> (inset in Figure 1a) displayed transparent structure, indicating ultrathin thickness. The typical high-resolution TEM (HRTEM) image of Ni-NSA-V<sub>Ni</sub> demonstrated a crystalline structure with a clear lattice spacing of 0.21 nm belonging to the (111) facet of Ni (Figure 1a). Some amorphous regions within the yellow circles could be clearly observed, indicating the presence of vacancies.<sup>35</sup> To exclude the influence of Ni substrate on the X-ray diffraction (XRD), Ni-NSA-V<sub>Ni</sub> was synthesized on Cu foam. The XRD pattern of Ni-NSA-V<sub>Ni</sub>/Cu (Figure 1b) exhibited exclusive signals of pure Ni (JCPDS no. 04-0850), which were the same as the Ni foam (Figure S3b).<sup>34</sup> Atomic force microscopy (AFM) image and the height configurations (Figure S4) revealed the thickness of Ni-NSA-V<sub>Ni</sub> as 1.8 nm, confirming their ultrathin thickness. X-ray photoelectron spectrum (XPS) and extended X-ray absorption fine structure (EXAFS) were performed to analyze Ni-NSA-V<sub>Ni</sub>. In Ni 2p XPS spectra (Figure 1c), the peaks at 852.9 and 870.3 eV could be assigned to Ni<sup>0</sup>, while two peaks of

855.6 and 873.5 eV arising from Ni<sup>2+</sup> could be ascribed to the unavoidable oxidation during XPS test.<sup>36</sup> The similarity of the Ni K-edge radial structure functions to that of the Ni foam verified that Ni-NSA-V<sub>Ni</sub> was metallic nickel (Figure 1d). The weaker peak intensity of Ni-Ni shell (2.4 Å) in Ni-NSA-V<sub>Ni</sub> compared to Ni foam arose from its decreased coordination number as a result of the nickel vacancies (Table S1).<sup>35</sup> The aforementioned results demonstrated that the H<sub>2</sub>-plasma treatment on Ni-NSA could produce abundant nickel vacancies with the maintaining of morphology and structure.

The performance of nitrite electroreduction was recorded versus the saturated calomel electrode (SCE) with 200 ppm nitrite-N (Figure 2). All electrochemical tests were performed in a standard three-electrode electrochemical cell by using 0.2 M Na<sub>2</sub>SO<sub>4</sub> solution as the electrolyte. A typical H-type electrolytic cell was used. The as-prepared samples on Ni foam, Pt plate and SCE were used as the working electrode, the counter electrode and the reference electrode, respectively. The reaction for calculation of conversion and Faradaic efficiency was operated for 2 hours. Colorimetric methods were adopted to determine the concentration of nitrite and ammonia in pre- and post-test electrolytes (Figure S5).<sup>9-11, 37-39</sup> The linear sweep voltammetry (LSV) curves of Ni-NSA-V<sub>Ni</sub> showed obvious enhancement in the current density in the presence of NaNO<sub>2</sub>, and the current density in Ni-NSA-V<sub>Ni</sub> was much higher than those of Ni foam (Figure S6 and Figure 2a).

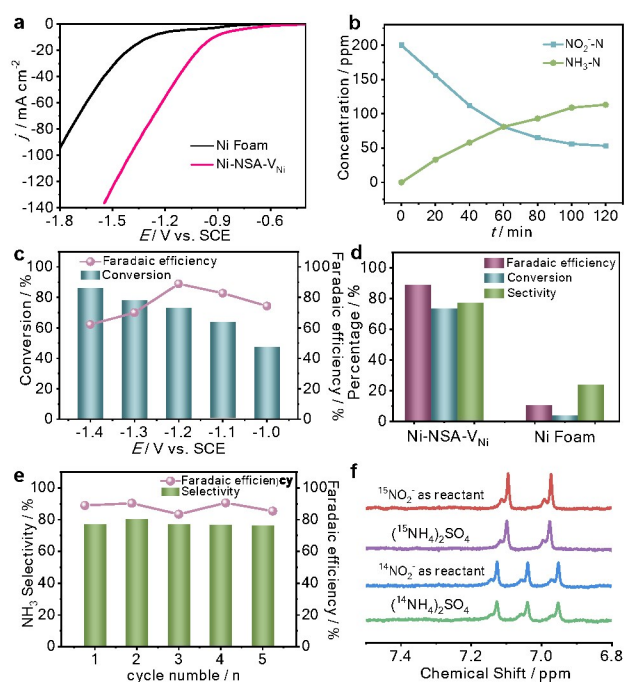


**Figure 2.** (a) LSV curves of Ni Foam and Ni-NSA-V<sub>Ni</sub> in 0.2 M Na<sub>2</sub>SO<sub>4</sub> with 200 ppm nitrite. (b) Time-dependent concentration of nitrite and ammonia over Ni-NSA-V<sub>Ni</sub> at -1.2 V vs. SCE. (c) Conversion yield of nitrite and Faradaic efficiency of ammonia over Ni-NSA-V<sub>Ni</sub> at different potentials. (d) Faradaic efficiency and selectivity of ammonia, and conversion rate of nitrite at -1.2 V vs. SCE. (e)

Selectivity and Faradaic efficiency of ammonia during consecutive recycling test for Ni-NSA- $V_{Ni}$  at -1.2 V vs. SCE. (f)  $^1H$  NMR spectra of standard samples ( $(^{15}NH_4)_2SO_4$  and  $(^{14}NH_4)_2SO_4$ ) and electrolyte after the  $NO_2^-$  reduction using  $^{14}NO_2^-$  and  $^{15}NO_2^-$  as N-source.

With prolonging the reaction time, the concentration of nitrite decreased, while the concentration of ammonia increased, suggesting nitrite reduction to ammonia (Figure 2b). The selectivity of ammonia over Ni-NSA- $V_{Ni}$  kept increase from -1.0 to -1.4 V, while the Faradaic efficiency displayed a volcanic shape curve with a maximum at -1.2 V (Figure 2c). Thus, we chose -1.2 V as the operation voltage for investigation on nitrite electroreduction. The electrocatalytic performance of Ni-NSA- $V_{Ni}$  (Conversion rate: 73.4%, Faradaic efficiency: 88.9%, Selectivity: 77.2%) was remarkably higher than those of Ni foam (Conversion rate: 10.8%, Faradaic efficiency: 3.9%, Selectivity: 23.9%) at -1.2 V vs. SCE (Figure 2d). Notably, the Faradaic efficiency and yield rate of ammonia were much higher than all the reported values of nitrogen electroreduction and among the best for electroreduction of nitrite into ammonia (Table S2). The electroreduction of 200 ppm nitrite in 2h was regarded as one cycle. The selectivity and Faradaic efficiency of ammonia exhibited no decay during five cycling tests (Figure 2e). Moreover, the morphology and structure of Ni-NSA- $V_{Ni}$  maintained well after the durability test, suggesting the high stability (Figure S7). The ignorable ammonia was detected without the addition of nitrite (Figure S8), indicating that the produced ammonia originated from nitrite reduction. Meanwhile,  $^{15}N$  isotope labelling experiments were conducted and the yield of ammonium was quantified by  $^1H$  nuclear magnetic resonance (NMR) spectra.<sup>40</sup> The  $^1H$  NMR spectra of electrolyte adopting  $^{15}NO_2^-$  as the reactant showed typical double peaks of  $^{15}NH_4^+$ , while the  $^1H$  NMR spectra of electrolyte adopting  $^{14}NO_2^-$  as the reactant displayed typical triple peaks of  $^{14}NH_4^+$  (Figure 2f).<sup>41, 42</sup> The  $^1H$  NMR results further confirmed that the produced ammonia derived from nitrite. For quantification, maleic acid ( $C_4H_4O_4$ ) was chosen as the  $^1H$  NMR external standard. Based on the standard curve of integral area ( $NH_4^+-N/C_4H_4O_4$ ) against  $NH_4^+-N$  concentration, the ammonia was quantified (Figures S9,10). The generated  $^{15}NH_4^+-^{15}N$  and  $^{14}NH_4^+-^{14}N$  quantified by  $^1H$  NMR were very close to the results quantified by colorimetric methods (Table S3), suggesting the quantitative accuracy.

To further probe the origin of high performance of Ni-NSA- $V_{Ni}$  for selective nitrite reduction to ammonia, a series of *in situ* and *ex situ* experiments and theoretical calculations were performed. First, the ammonia yield rate of Ni-NSA- $V_{Ni}$  was much higher than that of Ni foam (Figure 3a). Furthermore, the electrochemical impedance spectroscopy (EIS) results illustrated that vacancy-rich Ni-NSA- $V_{Ni}$  owned smaller interfacial charge-transfer resistance than Ni foam (Figure S11). Online differential electrochemical mass spectrometry (DEMS) measurement was performed for the detection of molecular intermediate and product over Ni-NSA- $V_{Ni}$  (Figure 3b).<sup>43-45</sup> The *m/z* signals of NO (30) and  $NH_3$  (17) combining with the large desorption free energies ( $\Delta G_{des}$ ) of NO on the surfaces of Ni foam ( $\Delta G_{des} = 2.53$  eV) and Ni-NSA- $V_{Ni}$  ( $\Delta G_{des} =$

2.61 eV) obtained by DFT calculations indicated NO as one of the intermediates. To gain insights into the nitrite electroreduction process, the surface electron cloud density and reaction Gibbs free energies ( $\Delta G$ ) were calculated based on DFT. Compared to Ni Foam, Ni-NSA- $V_{Ni}$  possessed lower surface electron cloud

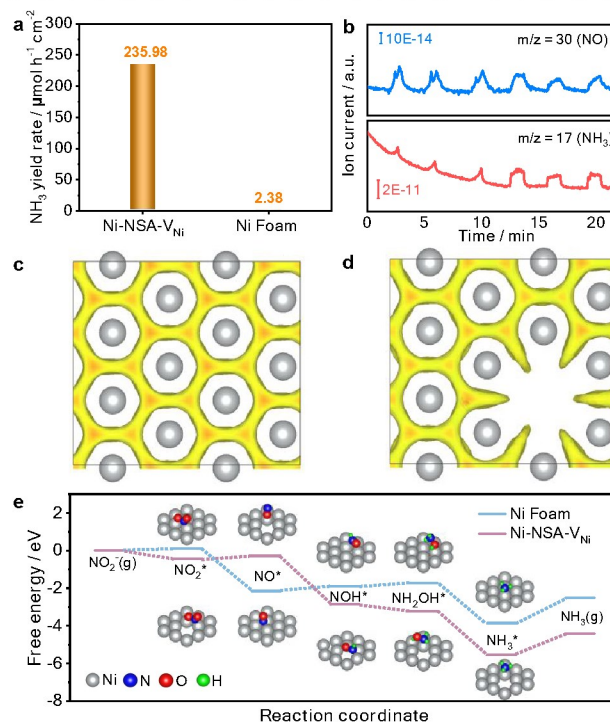


**Figure 3.** (a) The yield rate of ammonia over Ni Foam and Ni-NSA- $V_{Ni}$ . (b) DEMS of Ni-NSA- $V_{Ni}$  for nitrite electroreduction. Calculated surface electron density distribution of (c) Ni Foam and (d) Ni-NSA- $V_{Ni}$ . (e) Free energy diagram of the nitrite electroreduction process over Ni Foam and Ni-NSA- $V_{Ni}$  at 0 V vs. RHE.

density (Figures 3c,d). As displayed in Figure 3e, the adsorption energy of  $NO_2^-$  on Ni-NSA- $V_{Ni}$  (-0.44 eV) was much lower than that of Ni Foam (0.12 eV). For further hydrogenation processes, the reaction Gibbs free energy of each step was downhill or uphill with a small degree ( $\Delta G_{max} = 0.25$  and 0.16 eV over Ni Foam and Ni-NSA- $V_{Ni}$ , respectively), guaranteeing the conversion from  $NO_2^*$  to  $NH_3^*$ . The last desorption of  $NH_3$  from Ni-NSA- $V_{Ni}$  ( $\Delta G = 1.12$  eV) was also easier than that on Ni Foam ( $\Delta G = 1.34$  eV). Thus, the decreased surface electron cloud density in Ni-NSA- $V_{Ni}$  improved the adsorption and activation of  $NO_2^-$  and the desorption of  $NH_3$ , leading to high nitrite-to-ammonia catalytic performance over the Ni-NSA- $V_{Ni}$  cathode.

Next, the electrocatalytic semi-dehydrogenation of THIQs over Ni-NSA- $V_{Ni}$  anode was carried out in 1.0 M KOH aqueous solution. The 1,2,3,4-tetrahydroisoquinoline (**1a**) was selected as a model substrate. Without **1a**, OER proceeded on Ni-NSA- $V_{Ni}$  (Figure 4a). To achieve the current density of 50 mA  $cm^{-2}$  for OER, Ni-NSA- $V_{Ni}$  required 1.61 V vs. reversible hydrogen electrode (RHE). Notably, the oxidation peak before 1.45 V

arose from Ni<sup>II</sup>/Ni<sup>III</sup> redox, which was demonstrated as active species for the electrocatalytic semi-dehydrogenation conversion of THIQs.<sup>23</sup> After adding **1a**, Ni-NSA-V<sub>Ni</sub> exhibited increased current density, indicating the oxidation of THIQs (Figure 4a). Compared with Ni Foam (Figure S12), Ni-NSA-V<sub>Ni</sub> exhibited much higher current density, indicating the superior

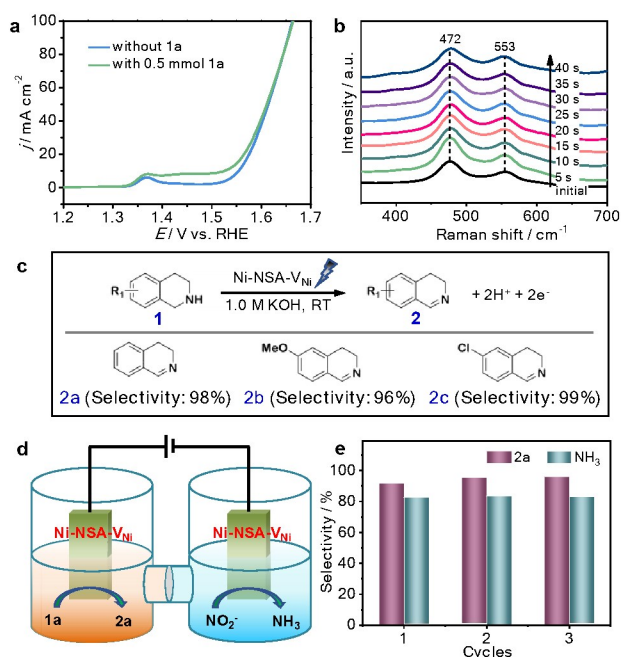


**Figure 4.** (a) LSV curves of Ni-NSA-V<sub>Ni</sub> anode at a scan rate of 5 mV s<sup>-1</sup> in 1.0 M KOH electrolyte with and without 0.5 mmol **1a**. (b) Time-dependent *in situ* Raman spectra of Ni-NSA-V<sub>Ni</sub> recorded at 1.4 V versus RHE in 0.1 M KOH solution without **1a** (initial) and after the addition of **1a**. (c) The substrate scope of the selective semi-dehydrogenation of THIQs over a Ni-NSA-V<sub>Ni</sub> anode. (d) Schematic illustration for coupling electrocatalytic semi-dehydrogenation of THIQs with nitrite electroreduction to ammonia. (e) Cycle-dependent selectivities of **2a** and ammonia over the Ni-NSA-V<sub>Ni</sub> bifunctional electrodes.

oxidation ability of THIQs. Time-dependent Raman spectra initially showed two peaks of NiOOH at 472 and 553 cm<sup>-1</sup> for Ni-NSA-V<sub>Ni</sub> (Figure 4b).<sup>23, 46</sup> The two peaks of NiOOH in Ni-NSA-V<sub>Ni</sub> maintained well after the addition of **1a**. This proved the superior stability of Ni<sup>II</sup>/Ni<sup>III</sup> species on Ni-NSA-V<sub>Ni</sub> during the electrooxidation process of **1a**. Ni-NSA-V<sub>Ni</sub> could efficiently drive a semi-dehydrogenation conversion of **1a** into **2a** with 98.0% selectivity and 95.5% Faradaic efficiency. 6-methoxy tetrahydroisoquinoline (**1b**) and hexachlorotetrahydroisoquinoline (**1c**) were efficiently converted to the corresponding dihydroisoquinolines with 96–99% selectivity, suggesting the good group tolerance of the tetrahydroisoquinoline semi-dehydrogenation over the Ni-NSA-V<sub>Ni</sub> anode (Figure 4c and Figure S13). Our results demonstrated that Ni-NSA-V<sub>Ni</sub> could act as the efficient bifunctional electrode materials for both cathodic nitrite-to-ammonia reduction and anodic tetrahydro-

isoquinoline semi-dehydrogenation. Thus, a Ni-NSA-V<sub>Ni</sub> || Ni-NSA-V<sub>Ni</sub> two-electrode electrolyzer was constructed to simultaneously produce ammonia at the cathode and DHIQs at the anode (Figures 4d). After adding **1a**, the current density increased for Ni-NSA-V<sub>Ni</sub>, indicating that the overall potential can be decreased by adopting oxidation of THIQs to replace OER (Figure S14). The selectivity of **2a** and ammonia over the Ni-NSA-V<sub>Ni</sub> bifunctional electrodes achieved 91.5% and 82.7% at the voltage of 1.5 V vs. counter electrode (CE). During continuous three cycles, no decrease in their selectivities was observed (Figure 4e), reflecting the good durability of the bifunctional Ni-NSA-V<sub>Ni</sub> electrodes. Although a great advance in using value-added reactions to replace OER in hydrogen production,<sup>18, 47–50</sup> this work is the first report on the development of high-value organic oxidation as an alternative anodic reaction at a low voltage in ammonia synthesis.

## Conclusions

In conclusion, we successfully introduced Ni vacancies into Ni nanosheets through the H<sub>2</sub>-plasma treatment. Ni vacancies could not only promote the cathodic selective nitrite electroreduction to ammonia (Faradaic efficiency: 88.9%, Selectivity: 77.2%), but also improve the anodic semi-dehydrogenation transformation of THIQs into DHIQs (Selectivity: 98.0%; Faradaic efficiency: 95.5%) over the Ni-NSA-V<sub>Ni</sub> electrodes. The combined results of *in situ* and *ex situ* experiments, and theoretical calculations revealed the enhanced mechanism of vacancies. The vacancies-induced decrease in the electronic cloud density of Ni improved the adsorption of NO<sub>2</sub><sup>-</sup> and the desorption of NH<sub>3</sub>, leading to high catalytic performance for nitrite reduction. Moreover, the Ni<sup>II</sup>/Ni<sup>III</sup> active species for the semi-dehydrogenation of THIQs maintained well during the electrooxidation process. Notably, the bifunctional Ni-NSA-V<sub>Ni</sub> electrodes can be assembled into a two-electrode electrolyzer for simultaneously producing ammonia and DHIQs with robust stability and high selectivity. This work opens a facile electrocatalytic strategy to integrate nitrite-to-ammonia reduction with the oxidative transformation of organic compounds with high efficiency.

## Conflicts of interest

There are no conflicts to declare.

## ACKNOWLEDGMENT

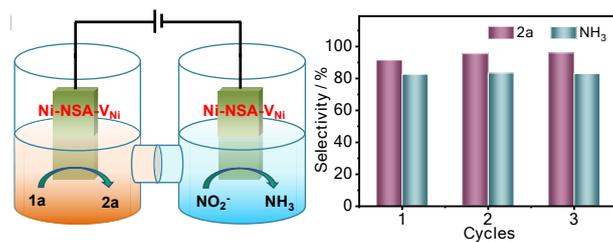
This work was financially supported by the National Natural Science Foundation of China (No. 22071173 and 21871206).

## References

- 1 S. G. Lehman, M. Badruzzaman, S. Adham, D. J. Roberts, D. A. Clifford, *Water Res.*, 2008, **42**, 969–976.
- 2 V. Rosca, M. Duca, M. T. de Groot, M. T. M. Koper, *Chem. Rev.*, 2009, **109**, 2209–2244.

- 3 H. Shin, S. Jung, S. Bae, W. Lee, H. Kim, *Environ. Sci. Technol.*, 2014, **48**, 12768-12774.
- 4 N. Singh, K. Patel, S. K. Sahoo, R. K. Pati, R. Kumar, *J. Mater. Chem. A*, 2017, **5**, 3389-3403.
- 5 Y. Matatov-Meytal, *Appl. Catal. B-Environ.*, 2003, **45**, 127-134.
- 6 M. Duca, S. Khamseh, S. C. Lai, M. T. Koper, *Langmuir*, 2010, **26**, 12418-12424.
- 7 H. Liu, X. Liu, Y. Yu, W. Yang, J. Li, M. Feng, H. Lia, *J. Mater. Chem. A*, 2018, **6**, 4611-4616.
- 8 D. He, Y. Li, H. Ooka, Y. K. Go, F. Jin, S. H. Kim, R. Nakamura, *J. Am. Chem. Soc.*, 2018, **140**, 2012-2015.
- 9 P. Wang, F. Chang, W. Gao, J. Guo, G. Wu, T. He, P. Chen, *Nat. Chem.*, 2017, **9**, 64-70.
- 10 J. Wang, L. Yu, L. Hu, G. Chen, H. Xin, X. Feng, *Nat. Commun.*, 2018, **9**, 1795.
- 11 C. Tang, S. Z. Qiao, *Chem. Soc. Rev.*, 2019, **48**, 3166-3180.
- 12 I. Ozturk, M. Altinbas, I. Koyuncu, O. Arikan, C. Gomec-Yangin, *Waste Manage.*, 2003, **23**, 441-446.
- 13 A. Thornton, P. Pearce, S. A. Parsons, *J. Hazard. Mater.*, 2007, **147**, 883-889.
- 14 M. H. Baryley, K. J. Takeuchi, T. J. Meyer, *J. Am. Chem. Soc.*, 1986, **108**, 5876-5885.
- 15 Y. Arikawa, Y. Otsubo, H. Fujino, S. Horiuchi, E. Sakuda, K. Umakoshi, *J. Am. Chem. Soc.*, 2018, **140**, 842-847.
- 16 Y. Guo, J. R. Stroka, B. Kandemir, C. E. Dickerson, K. L. Bren, *J. Am. Chem. Soc.*, 2018, **140**, 16888-16892.
- 17 M. W. Kanan, D. G. Nocera, *Science*, 2008, **321**, 1072-1075.
- 18 B. You, Y. Sun, *Acc. Chem. Res.*, 2018, **51**, 1571-1580.
- 19 M. Chaumontet, R. Piccardi, O. Baudoin, *Angew. Chem. Int. Ed.*, 2009, **48**, 179-182.
- 20 X. Cui, Y. Li, S. Bachmann, M. Scalone, A. E. Surkus, K. Junge, C. Topf, M. Beller, *J. Am. Chem. Soc.*, 2015, **137**, 10652-10658.
- 21 S. Kato, Y. Saga, M. Kojima, H. Fuse, S. Matsunaga, A. Fukatsu, M. Kondo, S. Masaoka, M. Kanai, *J. Am. Chem. Soc.*, 2017, **139**, 2204-2207.
- 22 M. Zheng, J. Shi, T. Yuan, X. Wang, *Angew. Chem. Int. Ed.*, 2018, **57**, 5487-5491.
- 23 C. Huang, Y. Huang, C. Liu, Y. Yu, B. Zhang, *Angew. Chem. Int. Ed.*, 2019, **58**, 12014-12017.
- 24 Y. Shi, B. Zhang, *Chem. Soc. Rev.*, 2016, **45**, 1529-1541.
- 25 J. Tian, Q. Liu, A. M. Asiri, X. Sun, *J. Am. Chem. Soc.*, 2014, **136**, 7587-7590.
- 26 T. Mitsui, M. K. Rose, E. Fomin, D. F. Ogletree, M. Salmeron, *Nature*, 2003, **422**, 705-707.
- 27 D. Yan, Y. Li, J. Huo, R. Chen, L. Dai, S. Wang, *Adv. Mater.*, 2017, **29**, 1606459.
- 28 Q. He, Y. Wan, H. Jiang, Z. Pan, C. Wu, M. Wang, X. Wu, B. Ye, P. M. Ajayan, L. Song, *ACS Energy Lett.*, 2018, **3**, 1373-1380.
- 29 C. Lv, Y. Qian, C. Yan, Y. Ding, Y. Liu, G. Chen, G. Yu, *Angew. Chem. Int. Ed.*, 2018, **57**, 10246-10250.
- 30 C. Li, Q. Yuan, B. Ni, T. He, S. Zhang, Y. Long, L. Gu, X. Wang, *Nat. Commun.*, 2018, **9**, 3702.
- 31 Q. Wang, Y. Lei, D. Wang, Y. Li, *Energy Environ. Sci.*, 2019, **12**, 1730-1750.
- 32 Y. Tong, P. Chen, M. Zhang, T. Zhou, L. Zhang, W. Chu, C. Wu, Y. Xie, *ACS Catal.*, 2017, **8**, 1-7.
- 33 Y. Zhu, X. Liu, S. Jin, H. Chen, W. Lee, M. Liu, Y. Chen, *J. Mater. Chem. A*, 2019, **7**, 5875-5897.
- 34 Y. Kuang, G. Feng, P. Li, Y. Bi, Y. Li, X. Sun, *Angew. Chem. Int. Ed.*, 2016, **55**, 693-697.
- 35 S. He, C. Li, H. Chen, D. Su, B. Zhang, X. Cao, B. Wang, M. Wei, D. G. Evans, X. Duan, *Chem. Mater.*, 2013, **25**, 1040-1046.
- 36 P. Prieto, V. Nistor, K. Nouneh, M. Oyama, M. Abd-Lefdil, R. Díaz, *Appl. Surf. Sci.*, 2012, **258**, 8807-8813.
- 37 L. S. Clesceri, A. D. Eaton, A. E. Greenberg, A. P. H. Association, A. W. W. Association, W. E. Federation, *American Public Health Association*, 1998.
- 38 M. Li, H. Huang, J. Low, C. Gao, R. Long, Y. Xiong, *Small Methods*, 2019, **3**, 1800388.
- 39 L. Li, C. Tang, B. Xia, H. Jin, Y. Zheng, S.-Z. Qiao, *ACS Catal.*, 2019, **9**, 2902-2908.
- 40 S. Z. Andersen, V. Colic, S. Yang, J. A. Schwalbe, A. C. Nielander, J. M. McEnaney, K. Enemark-Rasmussen, J. G. Baker, A. R. Singh, B. A. Rohr, M. J. Statt, S. J. Blair, S. Mezzavilla, J. Kibsgaard, P. C. K. Vesborg, M. Cargnello, S. F. Bent, T. F. Jaramillo, I. E. L. Stephens, J. K. Nørskov, I. Chorkendorff, *Nature*, 2019, **570**, 504-508.
- 41 Y. Wang, W. Zhou, R. Jia, Y. Yu, B. Zhang, *Angew. Chem. Int. Ed.*, 2020, **59**, 5350-5354.
- 42 L. Zhang, L. X. Ding, G. F. Chen, X. Yang, H. Wang, *Angew. Chem. Int. Ed.*, 2019, **58**, 2612-2616.
- 43 O. Wolter, J. Heitbaum, *Ber. Bunsenges. Phys. Chem.*, 1984, **88**, 2-6.
- 44 X. Wang, J. F. de Araujo, W. Ju, A. Bagger, H. Schmies, S. Kuhl, J. Rossmeisl, P. Strasser, *Nat. Nanotech.*, 2019, **14**, 1063-1070.
- 45 C. J. Bondué, F. Calle-Vallejo, M. C. Figueiredo, M. T. M. Koper, *Nat. Catal.*, 2019, **2**, 243-250.
- 46 Y. Huang, X. Chong, C. Liu, Y. Liang, B. Zhang, *Angew. Chem. Int. Ed.*, 2018, **57**, 13163-13166.
- 47 Y. Yuan, A. Lei, *Acc. Chem. Res.*, 2019, **52**, 3309-3324.
- 48 S. Barwe, J. Weidner, S. Cychy, D. M. Morales, S. Dieckhofer, D. Hiltrop, J. Masa, M. Muhler, W. Schuhmann, *Angew. Chem. Int. Ed.*, 2018, **57**, 11460-11464.
- 49 C. Tang, R. Zhang, W. Lu, Z. Wang, D. Liu, S. Hao, G. Du, A. M. Asiri, X. Sun, *Angew. Chem. Int. Ed.*, 2017, **56**, 842-846.
- 50 Z. Ji, J. Liu, Y. Deng, S. Zhang, Z. Zhang, P. Du, Y. Zhao, X. Lu, J. *Mater. Chem. A*, 2020, **8**, 14680-14689.

## TOC

View Article Online  
DOI: 10.1039/D0TA09590G

Ni nanosheet arrays with Ni vacancies exhibited outstanding electrocatalytic performances toward selective nitrite reduction to ammonia and semi-dehydrogenation of tetrahydroisoquinolines.